

Broadband antireflection film with moth-eye-like structure for flexible display applications

GUANJUN TAN,¹ JIUN-HAW LEE,² YI-HSIN LAN,² MAO-KUO WEI,³ LUNG-HAN PENG,² I-CHUN CHENG,² AND SHIN-TSON WU^{1,*}

¹College of Optics and Photonics, University of Central Florida, Orlando, Florida 32816, USA

²Graduate Institute of Photonics and Optoelectronics and Department of Electrical Engineering, National Taiwan University, Taipei, Taiwan

³Department of Materials Science and Engineering, National Dong Hwa University, Hualien, Taiwan

*Corresponding author: swu@ucf.edu

Received 17 January 2017; accepted 5 May 2017 (Doc. ID 285019); published 22 June 2017

Sunlight readability is a critical requirement for display devices, especially for mobile displays. Anti-reflection (AR) films can greatly improve sunlight readability by reducing the surface reflection. In this work, we demonstrate a broadband moth-eye-like AR surface on a flexible substrate, intended for flexible display applications. The moth-eye-like nanostructure was fabricated by an imprinting process onto a flexible substrate with a thin hard-coating film. The proposed nanostructure exhibits excellent AR with luminous reflectance <0.23% and haze below 1% with indistinguishable image quality deterioration. A rigorous numerical model is developed to simulate and optimize the optical behaviors. Excellent agreement between the experiment and simulation is obtained. Meanwhile, the nanostructure shows robust mechanical characteristics (pencil hardness >3 H), which is favorable for touch panels. A small bending radius (8 mm) was also demonstrated, which makes the proposed nanostructure applicable for flexible displays. Additionally, a fluoroalkyl coating was applied onto the moth-eye-like surface to improve the hydrophobicity (with a water contact angle >100°). Such a self-cleaning feature helps protect touch panels from dust and fingerprints. The proposed moth-eye-like AR film is expected to find widespread applications for sunlight readable flexible and curved displays. © 2017 Optical Society of America

OCIS codes: (220.4241) Nanostructure fabrication; (310.1210) Antireflection coatings; (310.6628) Subwavelength structures, nanostructures.

<https://doi.org/10.1364/OPTICA.4.000678>

1. INTRODUCTION

Sunlight readability is an important issue for mobile displays, whether it is a liquid crystal display (LCD) [1,2] or an organic light-emitting diode (OLED) display [3–5]. Mobile display devices are often used in outdoor environments, where strong sunlight reflected by the bare substrate surface would badly wash out the displayed images. To quantitatively evaluate the sunlight readability, the following ambient contrast ratio (ACR) has been commonly used [6,7]:

$$\text{ACR} = \frac{L_{\text{on}} + R_L \cdot L_{\text{ambient}}}{L_{\text{off}} + R_L \cdot L_{\text{ambient}}}, \quad (1)$$

where L_{on} and L_{off} are the luminance values of the on-state and off-state of a display, respectively, and L_{ambient} is the ambient luminance. R_L is the luminous reflectance of the display, defined by [5,7]

$$R_L = \frac{\int_{\lambda_1}^{\lambda_2} V(\lambda)R(\lambda)S(\lambda)d\lambda}{\int_{\lambda_1}^{\lambda_2} V(\lambda)S(\lambda)d\lambda}, \quad (2)$$

where $V(\lambda)$ is the spectral eye sensitivity defined by the CIE standard [8], $R(\lambda)$ is the reflectance of the display device, and $S(\lambda)$ is the

spectrum of the ambient light (CIE standard D65 source is used in this work). According to Eq. (1), the ACR decreases sharply as the ambient luminance increases. At the interface between the cover glass (refractive index ~1.5) and air, the Fresnel reflection is ~4%. Let us assume the display luminance is ~200 nits, under strong ambient conditions, e.g., brightness ~10⁴ nits for a typical sunny day; then, the calculated ACR is only ~1.5. That is to say, the displayed image is totally washed out.

To improve sunlight readability, a straightforward method is to boost the display luminance. A major tradeoff is increased power consumption. Another, more promising method is to reduce the surface reflection by laminating an anti-reflection (AR) and antiglare (AG) film on the display surface [9–13]. Indeed, the surface reflection can be reduced by the destructive interference through multilayer thin film coatings [10,11]. However, the reflection of such a multilayered structure is strongly dependent on the wavelength and incident angle of ambient light. Alternatively, bio-inspired moth-eye nanostructures exhibit excellent AR performance, with exceptional broadband wide-angle low reflectivity [12–15]. The moth-eye-like nanostructures have been utilized to enhance the photo-conversion efficiency of solar

cells [16–18] and to improve the sunlight readability of displays [13].

In this paper, we fabricated an AR moth-eye-like structure on a hard-coating thin film spun on a flexible polyethylene terephthalate (PET) and triacetyl cellulose (TAC) substrate for high-ACR flexible display applications. The moth-eye-like nanostructure exhibits an excellent AR property, with luminous reflectance $<0.23\%$. To understand the underlying physical mechanisms, we established a numerical model based on the finite element method (FEM) to fit the experimental data. Additionally, the haze of such nanostructured film was controlled under 1.5% in the visible region. To quantitatively estimate the image quality degradation, we took the Lena image on the same display with and without the nanostructure film attached and then calculated the universal image quality index. The results indicate that the image quality remains excellent, with an image quality index of 97% . For an interactive mobile display, a touch panel is usually embedded on the display. Therefore, a robust and self-cleaning outer surface of the touch panel is highly favorable. So, we adopted the hard-coating thin film for hardness enhancement. Generally speaking, a nanostructure is beneficial for improving the hydrophobicity. In our experiments, we employed the fluoroalkyl coating to further increase the self-cleaning characteristics. Our proposed nanostructure was fabricated by a self-assembling and imprinting process without further wet or dry etching. Hence, it has great potential for large-area and low-cost fabrication.

2. NANOSTRUCTURE FABRICATION

Figure 1 depicts the process flow of the moth-eye-like nanostructure fabrication. The first step was the oxygen plasma treatment on the glass substrate to get a hydrophilic surface. The SiO_2 spherical nanoparticles, with a diameter of ~ 100 nm, were dispersed in an aqueous solution and then spun on the pre-treated glass substrate to form a close-packed monolayer. The nanoparticle concentration was diluted to 8 wt. % for the spin-coating process. The nanoparticle spin coating was performed with spin speeds between $5000 \sim 6000$ rpm for 30 s. The process is quite reproducible with the spin-coating condition provided above [19]. Later, a close-packed nanoparticle monolayer was used as an imprinting template to transfer the nanostructure pattern to the hard-coating layer. The surface morphology of the template

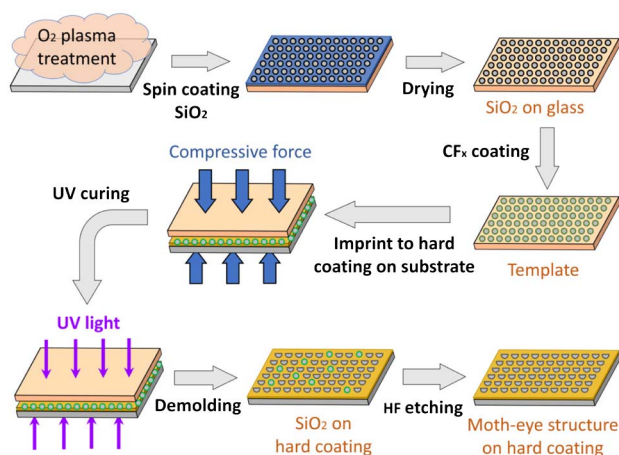


Fig. 1. Fabrication process flow of the moth-eye-like nanostructure on the hard-coating film above flexible PET or TAC substrate.

was characterized by scanning electron microscopy (SEM), and the microscopy image is shown in Fig. 2(a). From the SEM images, the particle diameter was measured to be 95.90 nm with a standard deviation of 5.88 nm, and the inter-particle distance was $12.49 \text{ nm} \pm 1.95$ nm. Actually, such a nanoparticle monolayer can also exhibit an AR property [20–24]. In our experiment, we used it as an imprinting template to obtain a concave structure. For alleviating the sticking problem between the SiO_2 nanoparticle and the hard-coating layer, CF_4 plasma treatment was employed to fluorinate the surface of the SiO_2 nanoparticles before the imprinting process. When the imprinting template was ready, we taped the flexible PET/TAC film on the other glass substrate for mechanical support. A UV-curable hard-coating material was spun on the PET/TAC film with a thickness of ~ 20 μm . The hard-coating material consists of liquid rubber, acrylate monomer, ethyl acetate, and a photo initiator, provided by Pro-Magic Corporation. Then, the PET/TAC film with the hard coating was contacted on the nanoparticle template with a compressive force of ~ 2204 gw/cm^2 . After imprinting, the hard coating was solidified by UV curing ($52 \text{ mW}/\text{cm}^2$ at 365 nm) for 10 min. The concave moth-eye-like structure appeared after the de-molding process, as shown in Fig. 2(b). We can see that there are still some nanoparticle residues on the hard-coating film, which can be etched off by an HF dipping process. Finally, the imprinted concave moth-eye-like structure was obtained.

Figures 2(c) and 2(d) show the top-view and side-view SEM images of the fabricated moth-eye-like structure on the hard-coating film. The fabricated concave nanostructured surface shows good large-area homogeneity. From the side-view image, more than half of the nanoscale sphere was pushed inside the hard-coating film during the nano-imprint process. Actually, the imprinting depth can be roughly estimated to be ~ 93 nm from the above SEM images. That led to nanosphere residue in the hard-coating film during the de-molding process. In order to enhance the self-cleaning behavior of the fabricated nanostructure, the surface of the moth-eye-like structure was fluorinated by thermally cured amphiphilic molecules (PMG-3199, produced by ProMagic Tech. Corp). The nanostructured surface was first

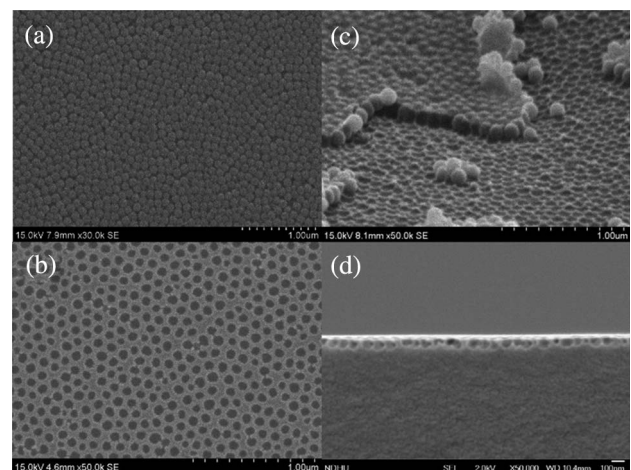


Fig. 2. SEM images of (a) SiO_2 nanoparticle monolayer on the template, (b) imprinted nanostructure on TAC substrate before HF dipping, (c) top view and (d) side view of final moth-eye-like nanostructure on TAC substrate.

treated by UV ozone to obtain hydrophilicity, followed by spin coating solutions containing amphiphilic fluoroalkyl-based molecules. After the removal of the solvent, the fluoro side was attached to the nanostructured surface, and the alkyl side provided a hydrophobic surface with great self-cleaning characteristics.

3. OPTICAL CHARACTERIZATION

In the optical characterization, we used a spectrophotometer (Hitachi U4100) to measure the spectra of the integrated transmittance, scattered transmittance, and reflectance of the fabricated nanostructure. By following the regulation of Japanese Industrial Standard (JIS) K7105, the haze spectra can be calculated from the integrated and scattered transmittance. The reflectance spectra of the moth-eye-like surface were measured by attaching the film to a calibrated black background.

As we discussed above, the template with the nanoparticle monolayer is also expected to have the AR characteristic. We first measured the optical behaviors of the template. Figure 3 shows the transmittance [Fig. 3(a)], reflectance [Fig. 3(b)], and haze [Fig. 3(c)] spectra of a planar glass substrate and the nanosphere-coated glass template. The maximum transmittance of the planar glass substrate reaches about 91.9% at 518 nm, according to Fig. 3(a). The interface between the air and the glass substrate (refractive index ~ 1.5) would result in $\sim 4\%$ reflection, which is consistent with the experimental result shown in Fig. 3(b). With the help of the nanosphere monolayer, the reflectance is obviously reduced, with a reflectance below 0.1% from 480 to 530 nm, which echoes the transmittance spectra in Fig. 3(a). Such a nanoparticle layer also leads to a slight increase in the haze spectra (1.09% at 400 nm). The nanosphere-coated

surface can provide excellent optical behaviors, but it usually suffers from low scratch resistance. Hence, we only use it as a template to obtain a robust AR film in our experiment.

Figures 3(d)–3(f) indicate the optical characteristics (transmittance, reflectance, and haze, respectively) of the PET substrate, planar hard-coating film on the PET substrate, and nanostructured hard-coating film on the PET substrate. The PET substrate we used in experiment was sandwiched by thin surface protection coatings. When the hard-coating material was coated above the surface coating on the PET substrate, the reflectance increases [Fig. 3(e)] due to the refractive index mismatch between the PET (~ 1.64), surface coating (~ 1.50), and the hard-coating (~ 1.48) layers. Figure 3(e) clearly illustrates that the moth-eye-like nanostructure helps reduce the reflectance. The minimum reflectance reaches $\sim 0.50\%$ at 515 nm, while the maximum transmittance increases to 96% at 503 nm correspondingly. The luminous reflectance was also calculated, according to Eq. (2), and the results are listed in Table 1. At the same time, the haze of moth-eye-like structure increases, as expected, but it still is lower than 1.3% from 400 to 750 nm. For the moth-eye-like nanostructure on the flexible TAC film [Figs. 3(g)–3(i)], an even better AR performance is observed. Less than 0.1% reflectance is obtained for wavelengths around 500 nm [Fig. 3(h)]. The luminous reflectance of the moth-eye-like structure on the TAC was 0.23%. The transmittance was improved to 95.4% [Fig. 3(g)], and the haze stayed lower than 1.5% in the visible region [Fig. 3(i)].

Figure 4 shows the pictures of three TAC films attached to a black background under the same white-light illumination. The bright spots are the images of the reflected light source. The reflections from the TAC substrate [Fig. 4(a)] and the planar

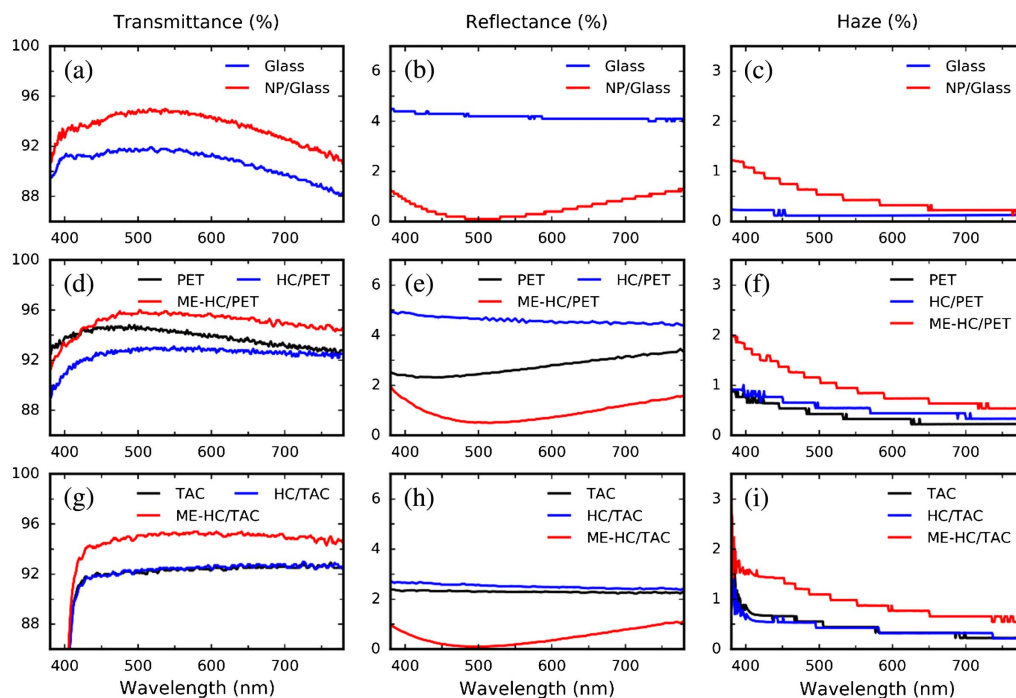


Fig. 3. Optical characterization results of the template and moth-eye-like nanostructures. Template: (a) transmittance, (b) reflection, and (c) haze spectra of glass substrate with and without SiO₂ nanosphere coating. Moth-eye-like structure on PET: (d) transmittance, (e) reflection, and (f) haze spectra of PET substrate, planar hard-coating film on PET substrate, and hard-coating film with moth-eye-like structure on PET substrate. Moth-eye-like structure on TAC: (g) transmittance, (h) reflection, and (i) haze spectra of TAC substrate, planar hard-coating film on TAC substrate, and hard-coating film with moth-eye-like structure on TAC substrate. (NP, nanoparticle; HC, hard coating; and ME, moth eye).

Table 1. Measured Transmittance (T), Reflection (R) and Haze (H) of the Films^a

	T_{\max} (%)	R_{\min} (%)	R_L (%)	H_{ave} (%)
Glass	91.90	4.00	4.18	0.13
NP/Glass	95.00	0.10	0.25	0.47
PET	94.80	2.31	2.63	0.37
HC/PET	93.10	4.43	4.59	0.52
ME-HC/PET	96.00	0.50	0.61	0.94
TAC	92.80	2.22	2.29	0.43
HC/TAC	93.00	2.39	2.51	0.41
ME-HC/TAC	95.40	0.10	0.23	0.95

^a(NP, nanoparticle; HC, hard coating; and ME, moth eye. Average range from 400 to 750 nm).

hard-coating film on the TAC substrate [Fig. 4(b)] are quite similar. For the moth-eye-like structure [Fig. 4(c)], the reflected intensity decreases, and the color becomes light magenta (because the reflection minimum is around 500 nm in the bluish-green region).

As shown in Fig. 3 and Table 1, the incorporation of the nanostructure inevitably leads to increased haze, which is also a drawback of the AG film. The image quality would also be deteriorated due to the haze. We can evaluate the image quality by the universal image quality index (Q), defined as [25]

$$Q = \frac{\sigma_{xy}}{\sigma_x \sigma_y} \times \frac{2\bar{x}\bar{y}}{\bar{x}^2 + \bar{y}^2} \times \frac{2\sigma_x \sigma_y}{\sigma_x^2 + \sigma_y^2}. \quad (3)$$

First, we should display the same image using the same display device, with and without the moth-eye-like nanostructured film. Then, the two images are captured by a camera, and the grayscale values of each pixel are extracted for the image quality calculation. In Eq. (3), $x = \{x_i | i = 1, 2, \dots, N\}$ and $y = \{y_i | i = 1, 2, \dots, N\}$ represent the grayscale values of each pixel of the original and test images. \bar{x} and \bar{y} are the averages, σ_x and σ_y are the standard deviations, and σ_{xy} is the covariance of x and y . The first, second,

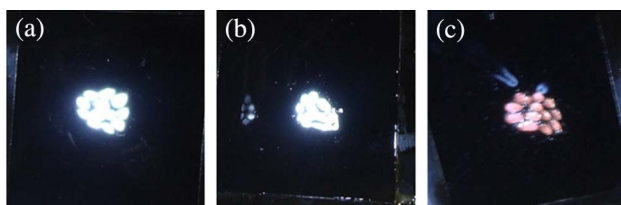


Fig. 4. Photographs of three films under the same white-light illumination. (a) TAC substrate, (b) planar hard-coating film on TAC substrate, and (c) hard-coating film with moth-eye-like structure on TAC substrate.

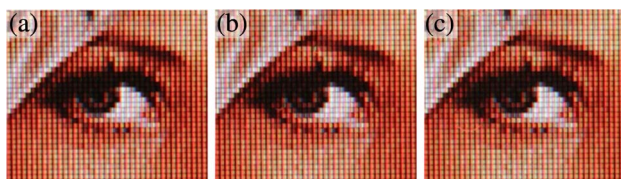


Fig. 5. Photos of Lena picture: (a) without, (b) with moth-eye-like nanostructured PET film, and (c) with moth-eye-like nanostructured TAC film attachment on the display.

and third terms in Eq. (3) describe the correlation, luminance difference, and contrast distortion of the two images, respectively. We laminated the nanostructured hard-coating TAC film onto the Lena picture. Figure 5 shows the camera-captured images. There is almost no image blur with the moth-eye-like film attached, even when the camera was zoomed in to a small part of the display. The calculated universal image quality indexes $Q = 0.9703$ for the moth-eye-like PET film and 0.9694 for the moth-eye-like TAC film, which are indistinguishable to the human eye.

4. OPTICAL SIMULATION

To understand the underlying mechanisms, we developed a numerical model to simulate the optical performance of the moth-eye-like nanostructured surface. The simulation model is based on FEM in the frequency domain with periodic boundary conditions. A schematic illustration of the simulated structure, including the nanostructured surface and coating layers, is shown in Fig. 6. The electromagnetic wave propagating through the moth-eye-like nanostructured surface needs to be simulated by FDTD or the FEM method [26–28]. As Fig. 6 indicates, the wave front after passing the nanostructure is still planar, which means the moth-eye-like surface can be treated as a planar surface in the later reflectance calculation. Next, the reflectance of nanostructured surface needs to be integrated into the multilayer structure reflectance calculation, as shown in Fig. 6. For the hard-coating and substrate layers, the thickness is much larger than the wavelength, which should be dealt with by the analytical wave propagation theory [29].

In our simulations, the refractive index is ~ 1.64 for PET, ~ 1.45 for TAC, and ~ 1.48 for the hard-coating film. The optical behaviors of the nanoparticle monolayer on the template, concave moth-eye-like surfaces on PET and TAC are simulated with the structure parameters obtained from the above SEM images. Figure 7 compares the experimental and simulated results for the reflectance of the concave moth-eye-like structures. Excellent agreement between the measurement and simulation is obtained. The moth-eye-like nanostructured hard coating on the PET film shows higher reflectance than the others, due to the index mismatch of the hard-coating and PET layers.

After having validated the numerical model, we are able to investigate the reflectance dependence on the structure parameters, for instance, the imprinting depth and particle diameter. Figure 8 depicts the simulated results of the moth-eye-like nanostructures with different parameters. For instance, Fig. 8(a) illustrates that the reflectance decreases as the imprinting depth increases. As for the diameter, the reflectance spectra indicate that the optimal

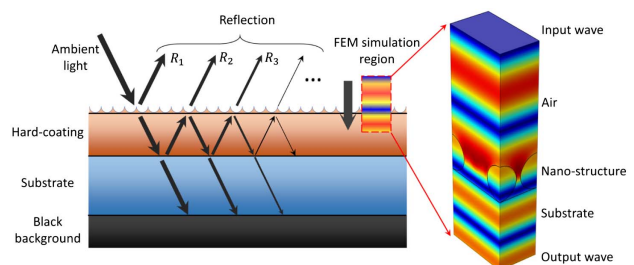


Fig. 6. Schematic illustration of the optical simulation of the moth-eye-like nanostructured films.

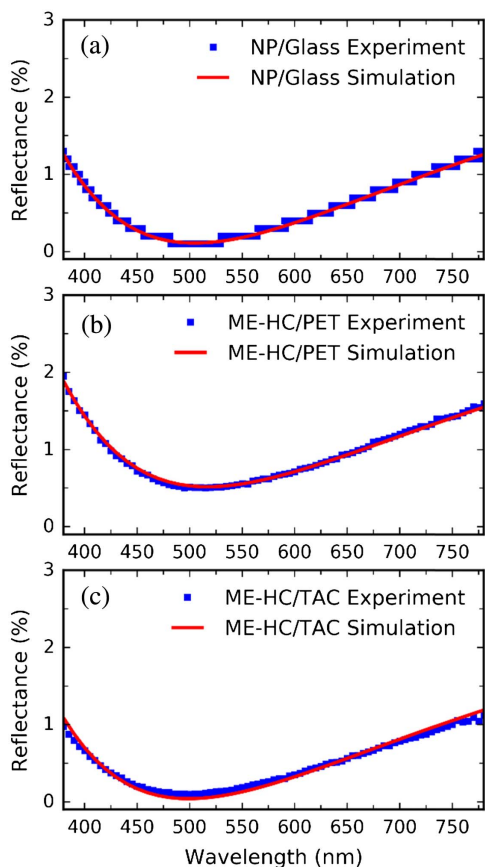


Fig. 7. Measured and simulated reflectance of nanostructured films: (a) nanoparticle template, (b) moth-eye-like nanostructured hard coating on PET film and (c) moth-eye-like nanostructured hard coating on TAC film.

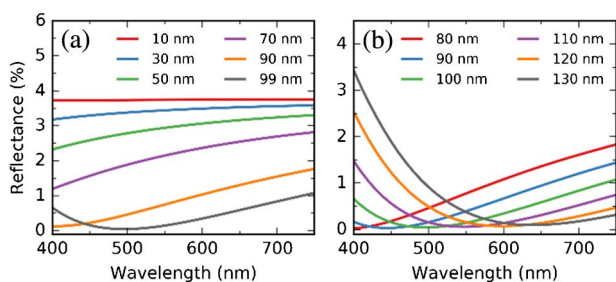


Fig. 8. Simulated reflectance spectra with different nanostructure parameters: (a) imprinting depth and (b) nanoparticle diameter.

nanoparticle diameter should be around 100 nm (green line), according to Fig. 8(b). Our model successfully explains the experimental results. It has been used to optimize the structure parameters for better optical performance.

5. MECHANICAL AND SURFACE CHARACTERIZATIONS

In addition to the optical performance, the mechanical properties of nanostructures are also very important [30] and need to be characterized. For a touch-panel interactive mobile device, high hardness of the touch surface is an important requirement.

Table 2. Mechanical Properties of Moth-Eye-Like Nanostructured Films

	Pencil Hardness	Flexibility
TAC	6 B	8 mm
HC/TAC	6 H	8 mm
ME-HC/TAC	3 H	8 mm

Table 2 lists the mechanical characteristics, including the hardness and bending radius, for the TAC substrate, planar hard-coating film on the TAC substrate, and nanostructured hard-coating film on the TAC substrate. A pencil hardness measurement was performed with a load of 500 g by a Mitsubishi pencil. After the pencil scraping, the sample was examined under the microscope according to the regulation of JIS K5600-5-4. The flexible TAC film is a soft material and is easily scratched with pencil hardnesses <6B. The hard-coating film helps to protect the surface, whose hardness can reach as high as 6 H. With the moth-eye-like nanostructure fabricated on the hard-coating film, the surface hardness decreases to 3 H.

Flexibility is a critical requirement for flexible displays. Our nanostructured surface exhibits a good flexibility as well. As shown in Table 2, those films passed the bending test with an 8-mm-diameter cylinder. In the flexibility test, we followed the procedures in JIS5600-5-1 (type 2) to measure the bending radius. The testing configuration is shown in Fig. 9. So, the moth-eye-like AR surface can be adopted in flexible and curved displays. Generally, the hardness of the hard-coating film can be adjusted by varying the concentrations of liquid rubber and acrylate. A higher acrylate concentration would lead to improved hardness but compromised flexibility. Hence, the tradeoff between hardness and flexibility should be balanced.

The touch panel surfaces are usually stained with fingerprints, skin oil, sweat, dust, and cosmetics. Such issues can be solved by using protective coating materials which possess hydrophobic and oleophobic properties [31,32]. The self-cleaning feature can protect touch panel surfaces from dust and fingerprints, which is quite favorable for touch panels. In order to improve the surface self-cleaning characteristic, we coated the nanostructured surface with amphiphilic fluoroalkyl-based molecules. The water contact angle is one of the criteria of the anti-fingerprint property [32]. Figure 10 illustrates the measurement of the water contact angle on the planar hard-coating and nanostructured hard-coating surfaces with an amphiphilic molecule coating. The water contact angle measurement was performed with the static sessile drop method. With the help of the nanostructure and the amphiphilic molecule coating, over a 100° contact angle can be achieved,

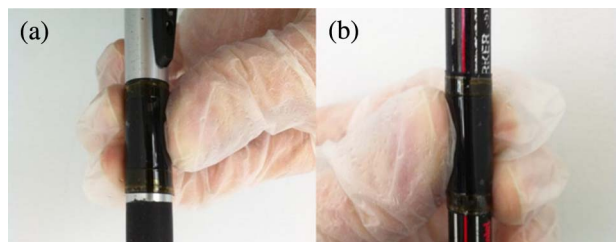


Fig. 9. Nanostructured films bending test configuration: (a) 12-mm-diameter cylinder and (b) 8-mm-diameter cylinder.

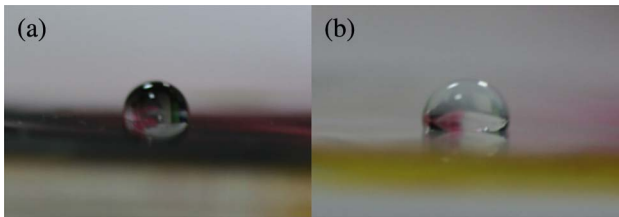


Fig. 10. Water contact angle measurement: (a) planar hard coating with contact angle 91.3° and (b) moth-eye-like structure on hard-coating film with contact angle 103.4° .

which means a good self-cleaning performance for such a nanostructure.

6. CONCLUSION

In summary, we have fabricated a broadband AR surface with a moth-eye-like structure for sunlight readable flexible display applications. The proposed nanostructure offers excellent optical properties, such as low luminous reflectance ($\sim 0.23\%$), high transmittance ($>95\%$), and low haze ($<1\%$). We also conducted a theoretical analysis by developing a numerical model based on the FEM. Excellent agreement between the simulation and experiment is obtained. The proposed nanostructure AR also exhibits high hardness, great flexibility, and self-cleaning characteristics. Such a moth-eye-like structure is expected to find widespread applications for sunlight readable flexible and curved display devices.

Funding. Air Force Office of Scientific Research (AFOSR) (FA9550-14-1-0279).

Acknowledgment. The UCF group is indebted to Yuge Huang for the helpful discussion and AFOSR for the partial financial support. The NTU group was supported by the Innolux Corporation.

REFERENCES

- H. H. Chung and S. Lu, "Contrast-ratio analysis of sunlight-readable color LCDs for outdoor applications," *J. Soc. Info. Disp.* **11**, 237–242 (2003).
- X. Zhu, Z. Ge, T. X. Wu, and S. T. Wu, "Transflective liquid crystal displays," *J. Display Technol.* **1**, 15–29 (2005).
- G. Trapani, R. Pawlak, G. R. Carlson, and J. N. Gordon, "High durability circular polarizer for use with emissive displays," U.S. patent 6,549,335 (15 April 2003).
- J. H. Lee, X. Zhu, Y. H. Lin, W. Choi, T. C. Lin, S. C. Hsu, H. Y. Lin, and S. T. Wu, "High ambient-contrast-ratio display using tandem reflective liquid crystal display and organic light-emitting device," *Opt. Express* **13**, 9431–9438 (2005).
- G. Tan, R. Zhu, Y. S. Tsai, K. C. Lee, Z. Luo, Y. Z. Lee, and S. T. Wu, "High ambient contrast ratio OLED and QLED without a circular polarizer," *J. Phys. D* **49**, 315101 (2016).
- J. A. Dobrowolski, B. T. Sullivan, and R. C. Bajcar, "Optical interference, contrast-enhanced electroluminescent device," *Appl. Opt.* **31**, 5988–5996 (1992).
- R. Singh, K. N. Narayanan Unni, and A. Solanki, "Improving the contrast ratio of OLED displays: An analysis of various techniques," *Opt. Mater.* **34**, 716–723 (2012).
- E. J. Schanda, *Colorimetry: Understanding the CIE System* (Wiley, 2007).
- A. M. Nuijs and J. J. L. Horikx, "Diffraction and scattering at antiglare structures for display devices," *Appl. Opt.* **33**, 4058–4068 (1994).
- N. Y. Kim, Y. B. Son, J. H. Oh, C. K. Hwangbo, and M. C. Park, "TiN_x layer as an antireflection and antistatic coating for display," *Surf. Coat. Technol.* **128**, 156–160 (2000).
- D. R. Gibson, I. Brinkley, and J. M. Walls, "Optical coatings and thin films for display technologies using closed-field magnetron sputtering," *Proc. SPIE* **5618**, 156–165 (2004).
- A. Chunder, K. Etcheverry, S. Wadsworth, G. D. Boreman, and L. Zhai, "Fabrication of anti-reflection coatings on plastics using the spraying layer-by-layer self-assembly technique," *J. Soc. Info. Disp.* **17**, 389–395 (2009).
- T. Taguchi, H. Hayashi, A. Fujii, K. Tsuda, N. Yamada, K. Minoura, A. Isurugi, I. Ihara, and Y. Itoh, "Ultra-low-reflective 60-in. LCD with uniform moth-eye surface for digital signage," *SID Symp. Dig. Tech. Pap.* **41**, 1196–1199 (2010).
- Y. F. Huang, S. Chattopadhyay, Y. J. Jen, C. Y. Peng, T. A. Liu, Y. K. Hsu, C. L. Pan, H. C. Lo, C. H. Hsu, Y. H. Chang, C. S. Lee, K. H. Chen, and L. C. Chen, "Improved broadband and quasi-omnidirectional anti-reflection properties with biomimetic silicon nanostructures," *Nat. Nanotechnol.* **2**, 770–774 (2007).
- B. Päivänranta, T. Saastamoinen, and M. Kuitinen, "A wide-angle anti-reflection surface for the visible spectrum," *Nanotechnology* **20**, 375301 (2009).
- N. Yamada, T. Ijro, E. Okamoto, K. Hayashi, and H. Masuda, "Characterization of antireflection moth-eye film on crystalline silicon photovoltaic module," *Opt. Express* **19**, A118–A125 (2011).
- T. G. Chen, P. Yu, Y. L. Tsai, C. H. Shen, J. M. Shieh, M. A. Tsai, and H. C. Kuo, "Nano-patterned glass substrates with different aspect ratios for enhanced light harvesting in a-Si:H thin film solar cells," *Opt. Express* **20**, A412–A417 (2012).
- J. Kim, A. J. Hong, J. W. Nah, B. Shin, F. M. Ross, and D. K. Sadana, "Three-dimensional a-Si:H solar cells on glass nanocone arrays patterned by self-assembled Sn nanospheres," *ACS Nano* **6**, 265–271 (2012).
- C. Y. Wang, L. Y. Chen, C. P. Chen, Y. W. Cheng, M. Y. Ke, M. Y. Hsieh, H. M. Wu, L. H. Peng, and J. Huang, "GaN nanorod light emitting diode arrays with a nearly constant electroluminescent peak wavelength," *Opt. Express* **16**, 10549–10556 (2008).
- H. Hattori, "Anti-reflection surface with particle coating deposited by electrostatic attraction," *Adv. Mater.* **13**, 51–54 (2001).
- Y. Zhao, J. Wang, and G. Mao, "Colloidal subwavelength nanostructures for antireflection optical coatings," *Opt. Lett.* **30**, 1885–1887 (2005).
- Z. Wu, J. Walish, A. Nolte, L. Zhai, R. E. Cohen, and M. F. Rubner, "Deformable antireflection coatings from polymer and nanoparticle multilayers," *Adv. Mater.* **18**, 2699–2702 (2006).
- K. Nakata, M. Sakai, T. Ochiai, T. Murakami, K. Takagi, and A. Fujishima, "Antireflection and self-cleaning properties of a moth-eye-like surface coated with TiO₂ particles," *Langmuir* **27**, 3275–3278 (2011).
- S. Ibuki, A. Matsumoto, M. Asahi, D. Wakizaka, N. Shibata, Y. Suga, and Y. Ito, "A novel moth-eye-like surface film that is anti-reflective and highly scratch resistant," *SID Symp. Dig. Tech. Pap.* **47**, 761–764 (2016).
- Z. Wang and A. C. Bovik, "A universal image quality index," *IEEE Signal Process. Lett.* **9**, 81–84 (2002).
- R. Dewan, S. Fischer, V. B. Meyer-Rochow, Y. Özdemir, S. Hamraz, and D. Knipp, "Studying nanostructured nipple arrays of moth eye facets helps to design better thin film solar cells," *Bioinspir. Biomim.* **7**, 016003 (2012).
- S. Ji, K. Song, T. B. Nguyen, N. Kim, and H. Lim, "Optimal moth eye nanostructure array on transparent glass towards broadband antireflection," *ACS Appl. Mater. Interfaces* **5**, 10731–10737 (2013).
- Y. W. Huang, W. T. Chen, W. Y. Tsai, P. C. Wu, C. M. Wang, G. Sun, and D. P. Tsai, "Aluminum plasmonic multicolor meta-hologram," *Nano Lett.* **15**, 3122–3127 (2015).
- O. S. Heavens, "Optical properties of thin films," *Rep. Prog. Phys.* **23**, 1–65 (1960).
- V. F. Chernov, H. Alaeian, J. A. Dionne, and J. R. Greer, "Polymer lattices as mechanically tunable 3-dimensional photonic crystals operating in the infrared," *Appl. Phys. Lett.* **107**, 101905 (2015).
- L. Y. Wu, S. K. Ngian, Z. Chen, and D. T. T. Xuan, "Quantitative test method for evaluation of anti-fingerprint property of coated surfaces," *Appl. Surf. Sci.* **257**, 2965–2969 (2011).
- A. Siriviriyanun and T. Imae, "Anti-fingerprint properties of non-fluorinated organosiloxane self-assembled monolayer-coated glass surfaces," *Chem. Eng. J.* **246**, 254–259 (2014).